

**Far-Infrared Constraints on Dust Shells
Around Vega-Like Stars**

Paul M. Harvey, Beverly J. Smith, James DiFrancesco, Cecilia Colomé
Department of Astronomy, The University of Texas at Austin
and Frank J. Low, Steward Observatory, University of Arizona

Received _____

Astrophysical Journal, in press

Abstract

We present results of observations at 47 and 95 μm from the Kuiper Airborne Observatory of several “Vega-like” stars. Spatial cuts and aperture photometry are presented for β Pictoris, Fomalhaut, and HD 135344, 139614, 142527, and 169142, four stars that had been suggested to possibly represent more distant examples of the Vega phenomenon by Walker and Wolstencroft. We have modelled the dust around β Pic and Fomalhaut with a spatially and optically thin disk to determine the constraints our new observations place on the properties of the dust disks that are required to explain the infrared and optical properties of these two stars. For β Pic we find that models similar to those proposed by Backman, Gillett, and Witteborn can fit our data quite well. For Fomalhaut we find that very different models are required which have much “blacker” dust with a much shallower density distribution, surface density $\propto r^{-0.5}$, than for β Pic. Our observations of the four HD stars are consistent with their being spatially unresolved. Because of their distance, this does not allow us to put any new constraints on their circumstellar shells.

1. Introduction

One of the most exciting and unexpected discoveries made by the IRAS survey was that of thermal dust emission from main-sequence stars, the “Vega” phenomenon (Aumann *et al.* 1984; Gillett 1986). Not only was dust unexpected around main sequence stars that were not undergoing detectable mass loss, but the cloud sizes and temperatures indicated that the particles must be much larger than typical interstellar grains. Furthermore, estimates of the lifetimes of such grains against radiation pressure and the Poynting-Robertson effect showed that the 10 to 100 μm diameter grains probably had to be constantly replenished from a reservoir of, perhaps, much larger grains. Unfortunately the spatial resolution of IRAS in the far-infrared, where these clouds are most luminous, was barely sufficient to resolve them. Therefore, the constraints on the dust properties due to the spatial extent of the clouds were not completely defined.

Immediately after the announcement of this discovery, the Kuiper Airborne Observatory was used to make both confirming observations of the phenomenon and to supply additional spatial and spectral constraints on the emission (Harvey, Wilking, and Joy 1984 (HWJ); Harper, Lowenstein, and Davidson 1984). These results as well as a recent re-analysis of the HWJ data (van der Bliik, Prusti, and Waters 1994) showed the value of the substantially higher spatial resolution possible with the KAO, even though its sensitivity is much poorer than that of IRAS.

For the past half-dozen years we have been attempting to obtain the highest possible quality new observations of several of these objects with the KAO. Since the largest fraction of them lie at southern declinations, this has involved the use of the KAO on its regular deployments to New Zealand which began with the

appearance of SN1987a. In this paper we report the results of these observations and discuss their implications for the properties of the circumstellar clouds around the observed stars. Our most complete data are on β Pictoris and Fomalhaut (α Piscis Austrinus). In addition, we have obtained some observations on four stars that were suggested by Walker and Wolstencroft (1988) to have properties similar to the four original stars found by IRAS. In the following sections of this paper we discuss: the details of our observations, the basic observational results, simple models that can fit most of the observational data on β Pic and Fomalhaut, and constraints on the dust shells around the additional stars.

2. Observations

All the observations presented here were made on the KAO flying out of Christchurch, New Zealand, between 1988 and 1994 with one of two detector systems. The first system consisted of an array of 1×8 bolometers imaged on the focal plane with a pixel scale of roughly $\lambda/2D \times \lambda/D$ at effective wavelengths of either 47 or 95 μm ($\lambda/\Delta\lambda \sim 1.5$) (Smith *et al.* 1991). The second system used the same optics, filtering, and pixel scale with a 2×10 array of bolometers (Smith *et al.* 1994). The details of the observations, including dates, calibration objects, detector system used, wavelengths, and objects observed are given in Table 1. Also shown in Table 1 is the rotational orientation of the sky relative to the detector arrays; for these angles the convention is that the long axis of each array was along the 0° - 180° line and the angle indicated is that by which the sky was apparently rotated from north (0°) through west (90°). All of the observed objects are bright, visible stars, so no off-axis guiding was required. The absolute calibrations are believed accurate to $\pm 15\%$, except in the case of the 1992 data where the large

number and consistency of calibration sources gives calibration uncertainties of $\pm 10\%$.

3. Observational Results

The results for all the objects observed are shown in Figures 1 - 4 and Table 2. The figures illustrate the spatial results and relevance of our flux density measurements to the overall energy distributions, and the table lists peak flux densities in our KAO beams relative to the IRAS large-beam results. Several of the figures also include modeling results that will be discussed below.

For β Pic it was impossible to schedule flights at a time when the orientation of our array would be along the major axis of the circumstellar disk. Therefore, our observations consist of peak flux measurements with the central pixel of the array (Table 2) together with measurements of several points 1/2 and 1 beamwidth on either side of the star along a line through the optical circumstellar disk (Figure 1, where all the measurements on either side have been averaged to improve the signal-to-noise ratio). The peak flux data (Table 2) show that at $95 \mu\text{m}$ the circumstellar cloud is marginally resolved in our KAO beam relative to the IRAS beam; at $47 \mu\text{m}$ there is clear evidence with our much smaller KAO beam that the cloud is resolved in the peak flux data; the $47 \mu\text{m}$ spatial data are also consistent with the idea that the source has been resolved, though they are certainly not compelling.

Our Fomalhaut data are summarized in Figure 3 and Table 2. The 1988 data are the only observations made with the long axis of our array essentially parallel to the IRAS in-scan direction along which the source appeared to be resolved by IRAS. All of the other $95 \mu\text{m}$ observations, as well as the only $47 \mu\text{m}$ observations, were made with the array roughly parallel to the IRAS cross-scan direction,

along which Fomalhaut showed no evidence for resolution by IRAS. As noted in a preliminary report on our first observations by Lester *et al.* (1988), our spatial data along the IRAS in-scan direction appear to resolve the circumstellar cloud at $95 \mu\text{m}$. In the perpendicular direction (all our other data), there is some evidence for resolution at $47 \mu\text{m}$, and slight evidence at $95 \mu\text{m}$. In the comparison of the peak flux measured in the KAO beam relative to the IRAS beams, however, Table 2 shows strong evidence that Fomalhaut is resolved in all the KAO observations assuming there has not been significant far-infrared variability over this time scale.

For the Walker and Wolstencroft objects all of the spatial data (Figure 4) are completely consistent with their circumstellar clouds being pointlike at the KAO resolution. The flux density results in Table 2, however, show that in two of the four observed cases, the $47 \mu\text{m}$ KAO flux measurements are lower than the IRAS fluxes by slightly more than the combined 1σ uncertainties in both. We do not consider this strong evidence for resolution of the clouds, but it suggests that there may be a small amount of emitting dust beyond the limits of the KAO beam.

4. Modeling

In order to compare our size information on these stars quantitatively with the IRAS data and to determine the implications of our data for the properties of the circumstellar clouds, we have tried fitting simple models to the available data. These models were designed to be similar to those that Backman, Gillett, and Witteborn (1992; hereafter BGW) constructed for β Pic, and we have extended them to Fomalhaut as well. The basic structure of the models assumes a spatially and optically thin disk. For β Pic the disk was assumed to be edge-on as suggested by the optical imagery; for Fomalhaut the inclination angle was allowed to vary. The circumstellar dust was assumed to be distributed in a single power-law

distribution between an inner and outer radius, or, for the most successful β Pic models, to have an inner distribution with one power-law, optical depth, and emissivity law, together with an outer distribution with different combination of power-law/ τ /emissivity. In these latter, two-component models, the radius dividing the two regions was fixed at the value used by BGW of 80 AU. The emissivity law for the dust in either component was characterized in a simple way; shortward of a specified wavelength, λ_o , the emissivity was assumed to be constant; longward of that wavelength it was assumed to decrease as either $\epsilon \propto \lambda^{-1}$ or $\epsilon \propto \lambda^{-2}$, although no models with a λ^{-2} dependence provided good fits to any of the data.

4.1. β Pic

Our aim in modeling β Pic was, first, to reproduce the results of BGW, and then to determine what additional constraints our data placed on their model results. BGW found that they were only able to fit the spectral and spatial data on β Pic with two-component models which had a substantially lower dust density distribution inside a radius of order 100 AU. They confirmed Gillett's conclusion that: (1) on average the grains around β Pic were smaller than those around Vega and Fomalhaut (i.e., $\lambda_o \sim \text{few } \mu\text{m}$), and (2) the inner radius for any thermally emitting dust, though model dependent, was of order 5 - 20 AU.

The additional constraints which we used from our data were the total flux densities measured in our KAO beams and the spatial data at 47 μm . Also, subsequent to BGW's paper, Zuckerman and Becklin (1993) published results of sub-mm photometry and mapping of β Pic and Fomalhaut. We have also included their 800 μm data, although small differences in the assumed emissivity law in the far-infrared can make almost any of the realistic models fit the 800 μm photometry.

The two best-fitting models of BGW were those labelled "10" and "11" in their paper. In both, the radius where the density changed from low to high was 80 AU,

and the surface density power-law was set at -1.7 in the outer region to match that inferred from the optical coronagraphy. The major differences in the two models were that model 10 used smaller grains and a larger inner radius to reproduce the shorter wavelength emission, and model 11 allowed a different power-law for the density gradient in the inner disk region but assumed identical grain properties in both regions. Because these provided the best fits to the data available to BGW, we attempted to fit our data as well as the previous data with one or both of these two models. Our results are shown in Figures 1 and 2 for a model we have labelled B10A which is quite similar to model 10 of BGW; we also found a model similar to their model 11 (which we called B11A) that gives comparable results which are not shown here. Figure 1 shows our spatial data relative to the model prediction; Figure 2 shows the model energy distribution, both total flux density, and flux density in various aperture sizes, including the IRTF 4" and 8" mid-infrared data discussed by BGW, our 47 and 95 μm KAO data, and Zuckerman and Becklin's 800 μm observations. Both models 10A and 11A provide a reasonable fit to all the data. The parameters for these models are listed in Table 3. We also confirmed that single density gradient models could not reproduce the observations. Two different regions with densities differing by a factor of 15 - 20 are required to produce enough far-infrared emission without overproducing the near-infrared emission and to fit the observed spatial extent in the 10 - 20 μm spectral region.

4.2. *Fomalhaut*

Gillett (1986) suggested simple models for the circumstellar clouds around the four original Vega-like stars to explain the IRAS photometry and scan data. For Fomalhaut he found that a distribution of black grains with a mild density gradient over a range of radii, 28 - 140 AU, gave a reasonable fit to the IRAS data. Therefore, we began our attempts to fit the IRAS, KAO, and sub-mm data

(Zuckerman and Becklin 1993) with a distribution of grains with $\lambda_o \sim 100 \mu\text{m}$ and a similar density gradient and range of radii. The facts that: (1) the IRAS in-scan and cross-scan source sizes were clearly different, and (2) that somewhat “accidentally” our KAO observations provided one dimensional source profiles roughly along the same directions as the IRAS data, suggested that we model the circumstellar cloud as an inclined disk. With no additional data or constraints on the disk inclination, nor the orientation of the IRAS or KAO scans relative to the disk, we have fit the data assuming that the IRAS in-scan data and 1988 KAO data were taken along the long axis of the source and that the IRAS cross-scan and subsequent KAO data were taken along the short apparent dimension. Because of this free parameter and the smaller quantity of spatial observations available than for β Pic, we concentrated our efforts on simple models with one dust density gradient and one type of dust between an inner and outer radius. This implies six free parameters for these models: surface density power-law, inner and outer radii, λ_o , optical depth, and inclination angle relative to the line of sight. For all the models we assumed a λ^{-1} emissivity law for $\lambda > \lambda_o$.

Figure 3 shows the results of the fits for the best model we found; the details of this model as well as models with other density gradients producing acceptable fits are listed in Table 4. The most important general features of models producing acceptable fits are: (1) a large range of radii over which a substantial amount of dust exists, (2) grains which have constant emissivity out to $\lambda \sim 100 \mu\text{m}$, and (3) inclination angles between 45° and 75° . (Because of the unknown orientation of the observations relative to the supposed disk, these values represent lower limits to the disk orientation). Surface density gradients, $\sigma \propto r^{-n}$, with $n \sim 0.5 \pm 0.5$ provide the only reasonably acceptable fits. Steeper gradients put too much flux into the KAO beam relative to the IRAS beam for models which reproduce the IRAS total fluxes; shallower density gradients have the opposite problem (as well as being difficult to

understand on physical grounds). A relatively large range in radii for the dust is needed to explain the decrease in flux observed with the KAO relative to IRAS; the derived range of inclination angles for the model disks is required to fit the differences in flux density observed in different array orientations on the KAO (as well as IRAS) and the spatial KAO data.

4.3. *Walker–Wolstencroft Stars*

We have not performed any detailed modeling to fit the data on these objects for the following reason. For all these stars which we observed, simple-minded models of circumstellar dust shells suggest that the shells should not be resolvable at the KAO limit even for dust grains with properties comparable to typical interstellar grains. For example, if we assume a single temperature dust shell whose temperature is determined by radiative equilibrium between power absorbed with efficiency, ϵ_a , and power radiated with efficiency, ϵ_r , the calculated diameter of the circumstellar shells for these four stars ranges from 3" for HD169142 to 10" for HD 142527 for a ratio $\epsilon_a/\epsilon_r = 100$, typical of normal interstellar grains at temperatures of $\sim 100\text{K}$. For blacker grains, the radius of a dust shell in thermal equilibrium would only be smaller than the above sizes, so we have no constraints on dust properties for grains in thermal equilibrium. Clearly, this also implies that if IRAS indeed resolved some of these dust shells, the extended emission must be due to faint, low level, extended dust which is cooler than the bulk of the dust contributing to the far-infrared fluxes reported by Walker and Wolstencroft (1988) (and confirmed by our KAO photometry). Perhaps a small number of tiny grains which are not in thermal equilibrium could explain the IRAS results.

5. Conclusions

The basic conclusion from our high-resolution work is that the models that explain the lower resolution IRAS data for β Pic and Fomalhaut are quite consistent with our higher-resolution KAO observations. Our most important conclusion for β Pic is that like BGW, we find that its circumstellar disk can be well fitted with a two component model whose main features are a substantially lower dust density inside ~ 100 AU and dust grains with a characteristic size of order a few microns. For Fomalhaut our most important conclusions are, first that we confirm Gillett's (1986) suggestion that the grains must be essentially black out to the longest wavelengths observed by IRAS and the KAO, $100 \mu\text{m}$. Secondly, the dust density gradient around Fomalhaut is probably in the range of $\rho \propto r^{-0.5 \pm 0.5}$. In addition, we find some evidence that Fomalhaut's circumstellar disk axis is likely to be inclined substantially to the line of sight, though the data do not seem consistent with an angle as high as that of β Pic. These conclusions show that the disks around β Pic and Fomalhaut are different in a number of important ways. In addition to Fomalhaut's being substantially lower optical depth (as are all the other related stars), there are large differences in particle size and in density gradient.

Our results on the four stars in Walker and Wolstencroft's list are difficult to reconcile with their analysis of the IRAS data which suggested that these stars have resolved dust shells in the far-infrared at the IRAS resolution of $\sim 1 - 2'$. With our KAO resolution of $10 - 20''$, these stars should have been easily resolved. Instead, we found them to be essentially point-like, both in the spatial cuts and by a simple comparison of KAO and IRAS flux densities. The observed dust temperatures and assumption of grain sizes even as small as typical interstellar grains do not require the dust shells to be large enough to be resolved by the KAO. Therefore, we cannot put any significant limits on the dust properties around these stars. On the other hand, the fact that we have not resolved them, even though they appeared to be in

the IRAS data, suggests that a careful search for faint, extended emission by ISO would be worthwhile.

Acknowledgments

We thank the staff of the KAO for their superb support during the number of years over which these observations were obtained. We hope that some of them will still be on the airborne astronomy team when SOFIA begins flying to make the next logical step in spatial resolution of these dust clouds.

References

- Aumann, H., Gillett, F.C., Beichman, C., DeJong, T., Houck, J., Low, F., Neugebauer, G., Walker, R., and Wesselius, P. 1984, *Ap.J. (Letters)*, **278**, L23.
- Backman, D.E., Gillett, F.C., and Witteborn, F.C. 1992, *Ap.J.*, **385**, 670.
- Gillett, F.C. 1986, in *Light on Dark Matter*, ed. Israel, F. (Dordrecht: Reidel), p.61.
- Harper, D.A., Loewenstein, R.F., and Davidson, J.A. 1984, *Ap.J.*, **285**, 808.
- Harvey, P.M., Wilking, B.A., and Joy, M. 1984, *Nature*, **307**, 441.
- Lester, D., Harvey, P., Smith, B., Colomé, C., and Low, F. 1990, *B.A.A.S.*, **21**, 1085.
- Smith, B.J., Lester, D.F., Harvey, P.M., and Pogge, R.W. 1991, *Ap.J.*, **373**, 66.
- Smith, B.J., Harvey, P.M., Colomé, C., Zhang, C.Y., Di Francesco, J., and Pogge, R.W. 1994, *Ap.J.*, **425**, 91.
- van der Blik, N.S., Prusti, T., and Waters, L.B.F.M. 1994, *Astr.Ap.*, **285**, 229.
- Walker, H.J., and Wolstencroft, R.D. 1988, *P.A.S.P.*, **100**, 1509.
- Zuckerman, B. and Becklin, E.E. 1993, *Ap.J.*, **414**, 793.

Table 1

Journal of Observations

Date	Calibrator	Detectors	λ (μm)	Star	Field Rot. ($^\circ$)
1988, Nov	Ceres, η Car	1×8	95	β Pic	290
			95	Fomalhaut	125
1989, Apr	Uranus, η Car	1×8	95	Fomalhaut	240
1990, May	Uranus, η Car	2×10	95	Fomalhaut	245
1991, Apr	Ceres, η Car	2×10	95	Fomalhaut	240
1992, Mar	Uranus, η Car,	2×10	47, 95	β Pic	115
	Callisto, Ceres, Neptune, Ganymede				
1993, Apr/May	Uranus, η Car	2×10	47, 95	Fomalhaut	250
				HD135344	95
				HD139614	90
1994, Jul/Aug	Uranus, η Car	2×10	47, 95	Fomalhaut	245
				HD135344	105
				HD142527	90
				HD169142	125

Table 2

Photometric Results

STAR	KAO F_ν (Jy) \pm stat. \pm total	@ λ	IRAS F_ν (Jy) @ λ	
β Pic	12.9	± 1.0 ± 1.6	@ $47\mu\text{m}$	18.8 ± 0.9 @ $60\mu\text{m}$
	8.5	± 0.6 ± 1.0	@ $95\mu\text{m}$	11.2 ± 1.0 @ $100\mu\text{m}$
Fomalhaut	5.6	± 0.65 ± 0.95	@ $47\mu\text{m}$	9.8 ± 0.5 @ $60\mu\text{m}$
	6.7	± 0.6 ± 1.0	@ $95\mu\text{m}$	11.3 ± 1.1 @ $100\mu\text{m}$
HD 135344	24.3	± 1.8 ± 3.5	@ $47\mu\text{m}$	26.3 ± 1.5 @ $60\mu\text{m}$
HD 139614	14.0	± 1.3 ± 2.5	@ $47\mu\text{m}$	18.3 ± 1.2 @ $60\mu\text{m}$
HD 142527	98	± 2.0 ± 15	@ $47\mu\text{m}$	106 ± 6 @ $60\mu\text{m}$
	84	± 1.2 ± 12	@ $95\mu\text{m}$	82 ± 5 @ $100\mu\text{m}$
HD 169142	22.9	± 2.1 ± 3.5	@ $47\mu\text{m}$	28.9 ± 2 @ $60\mu\text{m}$

Table 3 *β Pic Models*

Parameter	Model B10A	Model B11A
Incl. Angle	90°	90°
Inner Radius	20 a.u.	5 a.u.
Middle Radius	80 a.u.	80 a.u.
Outer Radius	2000 a.u.	2000 a.u.
γ (inner)*	-1.7	-0.4
γ (outer)*	-1.7	-1.7
λ_o (inner)	0.3 μm	2.5 μm
τ_{100} (inner)	2.9×10^{-4}	2.8×10^{-4}
τ_{100} (outer)	5.1×10^{-3}	5.0×10^{-3}
n**	-1	-1

*Surface density $\propto r^\gamma$; **Dust emissivity $\propto \lambda^n$

Table 4

Fomalhaut Models

Parameter	Best Model, #1	Model #2	Model #3
Incl. Angle	60°	65°	50°
Inner Radius	22 a.u.	16 a.u.	25 a.u.
Outer Radius	430 a.u.	300 a.u.	400 a.u.
γ^*	-0.5	0.0	-0.75
λ_o	80 μm	80 μm	85 μm
τ_{100}	2.7×10^{-5}	6.4×10^{-5}	5.6×10^{-5}
n^{**}	-1	-1	-1

*Surface density $\propto r^\gamma$; **Dust emissivity $\propto \lambda^n$

Figure Captions

Fig. 1 - Observational and model results for model B10A for β Pic. Dotted line - model spatial profile at infinite spatial resolution; dashed line - our KAO point source profile (PSP); solid line - model convolved with PSP; open triangles - observed average source brightness one-half and one beamwidth off center relative to the peak observed flux at $47 \mu\text{m}$. The error bars indicate the combined statistical and calibration uncertainties.

Fig. 2 - Model energy distributions for model B10A for β Pic relative to various observations. Our KAO observations are shown as open triangles close to the short-dashed line labelled “FIR” which is the model prediction for the flux in our finite size beams as well as for the $800 \mu\text{m}$ data of Zuckerman and Becklin (open triangle also). The 12, 25, 60 and $100 \mu\text{m}$ IRAS data are shown as open diamonds close to the solid line labelled “TOT” which is the model prediction for the total flux from the circumstellar disk. Other points close to the appropriate model lines for 4” and 8” apertures are taken from BGW. The error bars indicate the combined statistical and calibration uncertainties.

Fig. 3 - Model results for the best fit model described in the text and Table 4 for Fomalhaut together with various observations. The spatial scan panels show our observed 47 and $95 \mu\text{m}$ data relative to the model results, assuming that our (and the IRAS) data were taken exactly parallel and perpendicular to the disk axis. The KAO point-source-profiles are shown as dashed lines. The energy distribution panel shows the model results, both for the total flux, and for that contained within the KAO beam at 47 and $95 \mu\text{m}$ and the $800 \mu\text{m}$ beam of Zuckerman and Becklin (dotted).

The IRAS data are also shown close to (except at $12\ \mu\text{m}$) the solid, total flux line. The error bars indicate the combined statistical and calibration uncertainties.

Fig. 4 - Our observational spatial data on the four observed stars in the Walker and Wolstencroft list (points) relative to the point source profile (dash-dot line). None of these stars shows evidence for spatial resolution in these data. The error bars indicate the combined statistical and calibration uncertainties.

Authors' Addresses

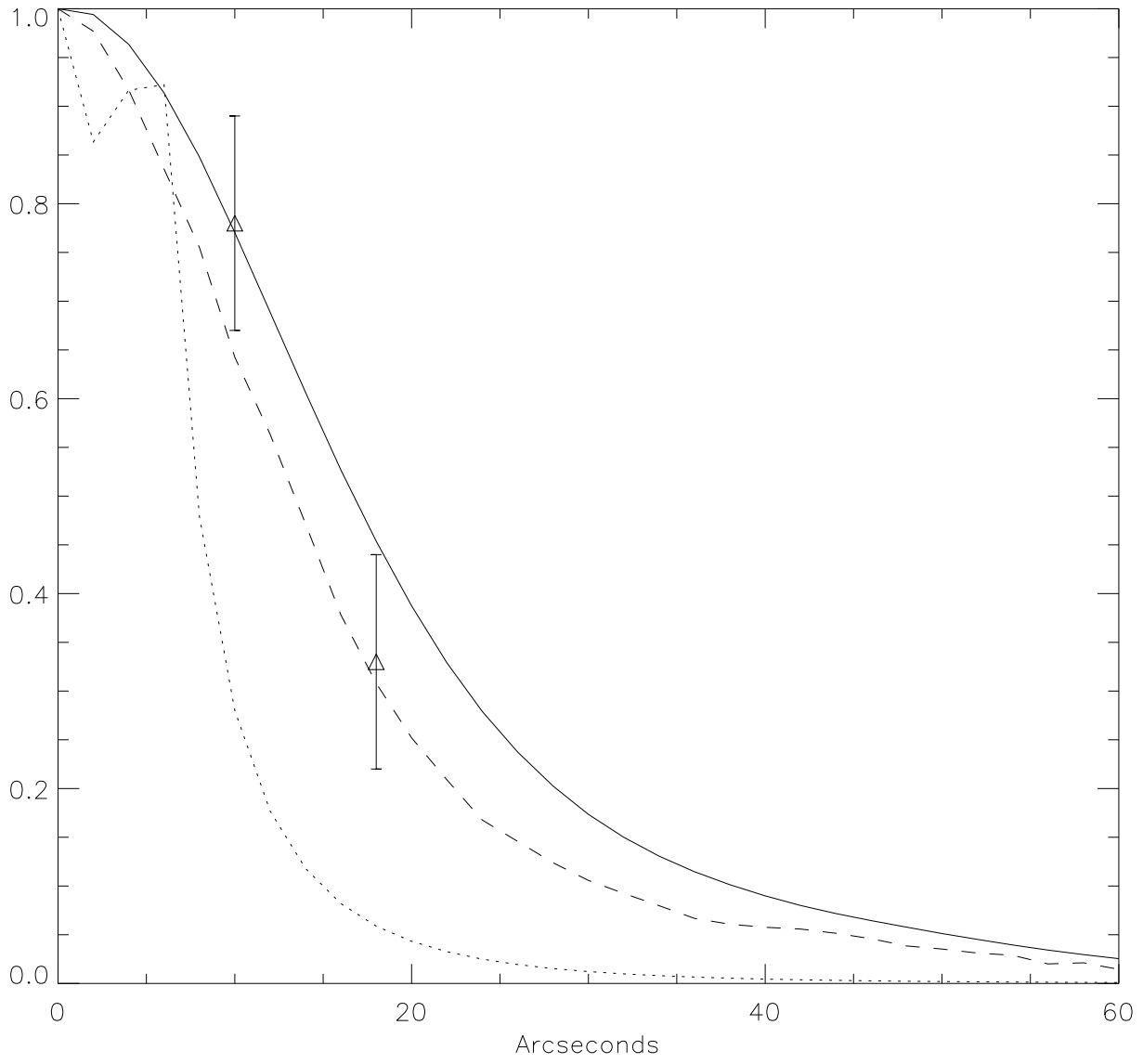
Paul M. Harvey, James Di Francesco, Astronomy Dept., University of Texas, Austin,
TX 78712

Beverly J. Smith, IPAC/Caltech, MS 100-22, Pasadena, CA 91125

Cecilia Colomé, Instituto de Astronomía, U.N.A.M., Apdo. Postal 70-264, DF-04510,
Mexico City, Mexico

Frank J. Low, Steward Observatory, University of Arizona, Tucson, AZ 85721

47um Normalized Beta Pic Profiles – Model B10A



Beta Pic Energy Distribution – Model B10A

